Journal of
Materials Chemistry B

COMMUNICATION

View Article Online
View Journal | View Issue

Cite this: J. Mater. Chem. B, 2019, 7, 4118

Received 3rd March 2019,
Accepted 29th May 2019

DOI: 10.1039/c9tb00435a

rsc.li/materials-b

Microporous organic network nanoparticles for dual chemo-photodynamic cancer therapy†

Dong Wook Kim,‡[a] Da Hye Kim,‡[b] June Young Jang,[a] Yoon-Joo Ko,[c] Sang Moon Lee,[d] Hae Jin Kim,[d] Kun Na *[b] and Seung Uk Son *[a]

This work shows that microporous organic network (MON) chemistry can be applied to the dual photodynamic and chemical therapy of cancer cells. Water-compatible and Zn-phthalocyanine (ZnPhT) loaded MON nanoparticles were engineered through size-controlled synthesis using poly(vinylpyrrolidone) (PVP) as a surfactant, followed by postsynthetic sulfonation of materials. The ZnPhT was successfully loaded on the sulfonated MON nanoparticles (N-SMONs) *via* coulombic interaction between anionic sulfonate and cationic ZnPhT. Because of their microporosity and high surface area, DOX was loaded efficiently on the ZnPhT/N-SMON nanoparticles. The resultant DOX/ZnPhT/N-SMON showed synergistic performance in the dual photodynamic and chemotherapy of cancer cells and tumors in *in vitro* and *in vivo* tests.

Recently, various microporous organic networks (MONs) have been synthesized through the coupling reactions of organic building blocks.[1] For example, the Cooper research group has shown that various MONs can be prepared by the Sonogashira coupling of multiethynyl arenes and multihalo arenes.[2] The key features of MONs are their high surface area, microporosity, and chemical stability.[1] Based on these features, MONs have been applied for gas storage or as adsorbents.[1,3] While MONs can be considered as promising drug delivery materials, the related studies are in the early stage.[4]

For the application of MONs to drug delivery for cancer therapy, two additional features are required. First, the water-compatibility of the MONs should be achieved. Usually, MONs prepared by the Sonogashira coupling of conventional organic building blocks have shown a superhydrophobic feature.[5] Thus, in order to obtain water-compatible MONs, additional functional groups and water-compatible moieties should be incorporated.[6] Second, size-controlled MONs should be achieved.[7] Usually, MONs have been obtained as powders with irregular morphologies and micron sizes. However, the performance of drug delivery materials is dependent on their sizes.[8] It has been well documented that nanoparticles have shown much longer circulation periods because of their lower uptake by the reticuloendothelial system.[8] In addition, because tumors grow relatively fast, the microenvironments of tumors are coarse and nanoporous.[8] Due to the enhanced permeability and retention (EPR) effect,[9] nanoparticles are known to easily access tumors and show high intratumoral accumulation.[8] In this regard, the size of MONs should be controlled to be nanoscale so that they can serve as efficient drug delivery systems for tumor therapy.

Recently, a dual strategy of cancer therapy has been studied.[10] Cancer cells have heterogeneous microenvironments and properties, and can thus show heterogeneous responses against therapy. Therefore, dual cancer therapy is expected to improve the efficiency of treatment. Over the last several decades, photodynamic therapy (PDT) for tumors has been extensively studied. As representative systems, porphyrins or phthalocyanines have been used for PDT.[11] On the other hand, there has been much progress on chemotherapy for tumors using drugs such as doxorubicin (DOX).[12] The combination of PDT with chemotherapy can be one of the efficient approaches for cancer treatment. Although the MONs have been recently applied for drug delivery, as far as we are aware, there have been no reports on multi-functional MON-based systems for dual cancer therapy.[4] In this work, we report the chemical engineering of water-compatible MON nanoparticles, the grafting of Zn-phthalocyanines to the MON nanoparticles for PDT, and their DOX delivery performance for dual cancer therapy.

Fig. 1 shows the synthetic strategy for the Zn-phthalocyanine loaded MON nanoparticles (ZnPhT/N-SMON). In the presence

[a] Department of Chemistry, Sungkyunkwan University, Suwon 16419, Korea. E-mail: sson@skku.edu
[b] Department of Biotechnology, The Catholic University of Korea, Bucheon 14662, Korea. E-mail: kna6997@catholic.ac.kr
[c] Laboratory of Nuclear Magnetic Resonance, National Center for Inter-University Research Facilities (NCIRF), Seoul National University, Seoul 08826, Korea
[d] Korea Basic Science Institute, Daejeon 34133, Korea

† Electronic supplementary information (ESI) available: Experimental procedures, additional characterization data, and *in vivo* studies of MON materials. See DOI: 10.1039/c9tb00435a

‡ These authors contributed equally.

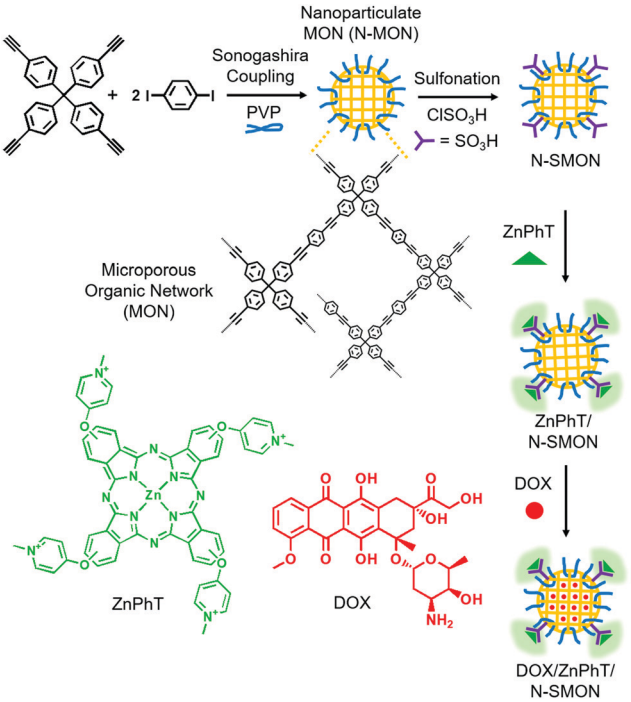

Fig. 1 The synthetic strategy for ZnPhT/N-SMON as a DOX carrier and for dual cancer therapy.

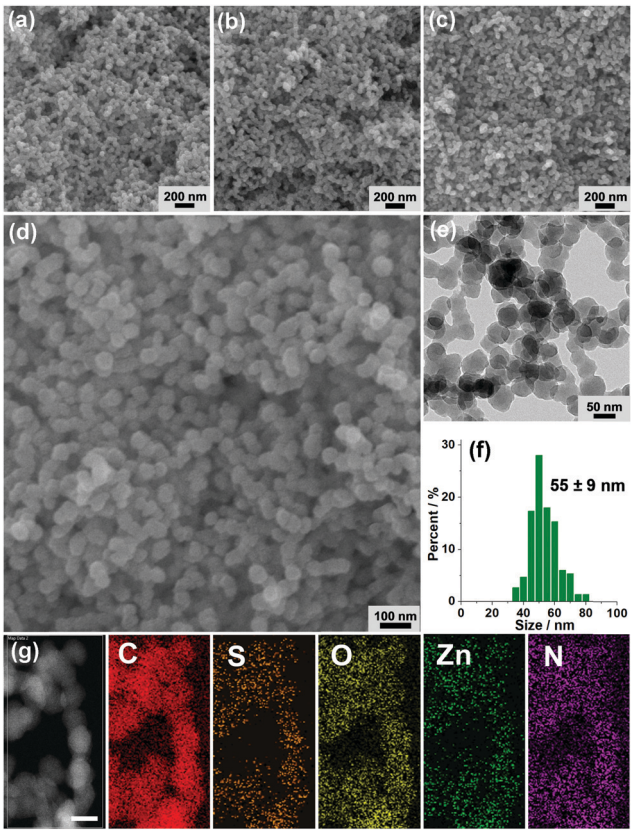

Fig. 2 SEM images of (a) N-MON, (b) N-SMON, and (c and d) ZnPhT/N-SMON. (e) TEM image, (f) size distribution diagram, and (g) TEM-EDS elemental mapping images (scale bars = 50 nm) of ZnPhT/N-SMON.

of poly(vinylpyrrolidone) (PVP), the Sonogashira coupling of tetra(4-ethynylphenyl)methane[13] with 1,4-diiodobenzene resulted in nanosized MON particles (N-MON). During the formation of networks, the water soluble PVP chains were entrapped into the networks of N-MON, resulting in water-compatible organic nanoparticles. Through the sulfonation of N-MON particles with $ClSO_3H$, sulfonic acid groups were incorporated into the materials to form N-SMON particles.[14] It has been reported that sulfonic acid is an efficient anchoring group for cationic molecules *via* the coulombic interaction between sulfonate and the cationic guests.[15] In this regard, a Zn-phthalocyanine with pyridinium salts (ZnPhT) was prepared[16] and loaded onto the N-SMON to form ZnPhT/N-SMON. The loaded ZnPhT in the ZnPhT/N-SMON could not be removed by simple washing with methanol or water.

Fig. 2 shows the morphology and size analysis of the materials by scanning (SEM) and transmission electron microscopy (TEM). The SEM image of N-MON showed a nanoparticulate morphology (Fig. 2a). The original morphology of N-MON was maintained in the SEM images of N-SMON and ZnPhT/N-SMON (Fig. 2b–d). Based on the TEM analysis, the average diameter of ZnPhT/N-SMON was measured to be 55 ± 9 nm (Fig. 2e and f). The hydrodynamic diameter of ZnPhT/N-SMON was measured to be 72 nm in water by dynamic light scattering (Fig. S1 in the ESI†). The elemental mapping of ZnPhT/N-SMON nanoparticles based on energy dispersive X-ray spectroscopy (EDS) showed a homogeneous distribution of zinc, nitrogen, and sulfur over the materials, indicating the successful incorporation of sulfonic acids and Zn-phthalocyanines (Fig. 2g).

According to the analysis of N_2 adsorption–desorption isotherm curves based on the Brunauer–Emmett–Teller theory, the N-MON showed a surface area of 469 $m^2\ g^{-1}$ (Fig. 3a). Through the sulfonation, the surface area of N-SMON was decreased to 366 $m^2\ g^{-1}$, matching with the conventional trends observed in the post sulfonation of MON materials in the literature.[14,15] The loading of ZnPhT resulted in a further decrease of the surface area of ZnPhT/N-SMON to 281 $m^2\ g^{-1}$. Pore size distribution analysis based on the density functional theory method showed that all N-MON, N-SMON, and ZnPhT/N-SMON materials have microporosity (pore sizes < 2 nm) (Fig. 3a).

The chemical structures of the materials were characterized by infrared absorption (IR) and solid state ^{13}C nuclear magnetic resonance (NMR) spectroscopy. The IR spectrum of N-MON showed aromatic C=C and C–H vibration peaks at 1508 and 818 cm^{-1}, respectively (Fig. 3b). In addition, the C=O vibration of the entrapped PVP was observed at 1673 cm^{-1}. The N-SMON showed additional S=O and O–H vibration peaks of sulfonic acid groups at 1208 and 3463 cm^{-1}, respectively.[14] While the zeta potential of N-MON was measured to be −12.5 mV, and that of N-SMON was measured to be −34.4 mV, indicating the successful incorporation of sulfonic acid groups. In comparison, ZnPhT/N-SMON showed the zeta potential of −25.1 mV due to the loading of cationic ZnPhT (Fig. S1 in the ESI†). In the IR spectrum of ZnPhT/N-SMON, although a minor peak of

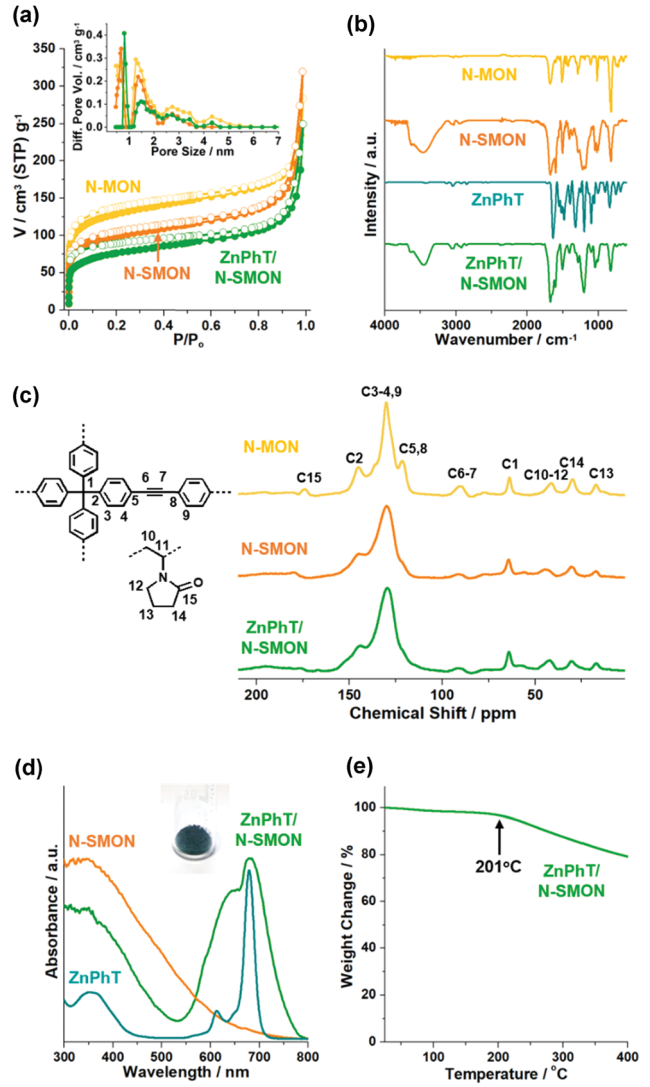

Fig. 3 (a) N_2 adsorption–desorption isotherm curves obtained at 77 K and pore size distribution diagrams based on the DFT method, (b) IR absorption spectra, and (c) solid state ^{13}C NMR spectra of N-MON, N-SMON, and ZnPhT/N-SMON. (d) UV/vis absorption spectra of N-SMON, ZnPhT, and ZnPhT/N-SMON and a photograph of ZnPhT/N-SMON. (e) A TGA curve of ZnPhT/N-SMON.

ZnPhT was observed at 1101 cm^{-1}, the vibration peaks of ZnPhT were not clearly distinguished from those of N-SMON, due to the minor amount of ZnPhT in the ZnPhT/N-SMON.

The solid state ^{13}C NMR spectrum of N-MON showed the ^{13}C peaks of benzyl carbon and internal alkynes at 64 and 90 ppm, respectively (Fig. 3c). The aromatic ^{13}C peaks of N-MON appeared at 121, 130, 136, and 145 ppm. In addition, the ^{13}C peaks of the entrapped PVP were observed at 17, 29, 41, and 174 ppm. Compared with N-MON, the N-SMON showed a significant change of aromatic ^{13}C peaks, indicating the incorporation of sulfonic acid groups into aromatic moieties in the materials.[13,14] The ^{13}C NMR spectrum of ZnPhT/N-SMON was similar to that of N-SMON, due to the minor amount of ZnPhT in the ZnPhT/N-SMON. Based on the elemental analysis of nitrogen (1.78 wt%) of N-MON, the content of PVP in the N-MON was measured to be 14 wt%. The content of sulfonic acids in the N-SMON was measured to be 1.70 mmol g^{-1} based on the content of sulfur (5.45 wt%). Supposing that the change in nitrogen content between N-SMON (0.78 wt%) and ZnPhT/N-SMON (3.11 wt%) resulted from the loading of cationic ZnPhT, the content of ZnPhT in the ZnPhT/N-SMON was measured to be 0.14 mmol g^{-1} (14.7 wt%).

The loading of ZnPhT on the N-SMON was further confirmed by UV-vis absorption spectroscopy. The N-SMON showed a dark brown color with a maximum absorption band at 351 nm (Fig. 3d). The ZnPhT had a deep green color with major absorption bands at 612 and 680 nm.[16] The ZnPhT/N-SMON showed a deep green color with major absorption bands at 643 and 681 nm, indicating the successful loading of ZnPhT onto the N-SMON. The results of thermogravimetric analysis (TGA) showed that the ZnPhT/N-SMON is thermally stable up to 201 °C (Fig. 3e). Powder X-ray diffraction (PXRD) study revealed that N-MON, N-SMON, and ZnPhT/N-SMON are all amorphous, matching with the conventional features of MON materials prepared by Sonogashira coupling in the literature[2] and indicating that the ZnPhT was distributed over the N-SMON materials without crystalline packing (Fig. S2 in the ESI†).

According to the measurement of water contact angle (WCA), the water-compatibility of the materials gradually increased from N-MON (WCA of 55°) to N-SMON (WCA of 23°) and ZnPhT/N-SMON (WCA of 13°) with an increase of water-compatible components such as PVP, sulfonate, and cationic ZnPhT. Water drops were eventually absorbed into the N-MON, N-SMON, and ZnPhT/N-SMON materials after 35, 4, and 0.2 s, respectively (Fig. 4a). The aqueous suspensions of the N-MON, N-SMON, and ZnPhT/N-SMON were quite stable for a week without forming aggregates (Fig. S3 in the ESI†). Moreover, the ZnPhT was not leached from ZnPhT/N-SMON for a week in phosphate buffered saline solution (PBS, pH 7.4) and in model blood solution at 37 °C, possibly due to the multi-site coulombic interaction between sulfonates of N-SMON and pyridiniums of ZnPhT (Fig. S4 and S5 in the ESI†). In addition, the ZnPhT/N-SMON maintained the original particulate morphologies for a week in model blood solution at 37 °C (Fig. S5 in the ESI†). Considering the microporosity and water-compatibility of ZnPhT/N-SMON, we studied its doxorubicin (DOX) delivery performance for dual photodynamic and chemo cancer therapy. Fig. 4b–f, 5, and 6 summarize the results.

First, the singlet oxygen generation ability of ZnPhT/N-SMON was studied (Fig. 4b). As the laser irradiation (671 nm) energy increased from 0.5 J cm^{-2} to 4 J cm^{-2}, the emission of 9,10-dimethylanthracene (DMA) was completely quenched *via* a reaction of DMA with the singlet oxygen produced by ZnPhT/N-SMON. In addition, as the concentration of ZnPhT/N-SMON increased from 20 μg mL^{-1} to 80 μg mL^{-1}, the singlet oxygen generation was enhanced, indicating that the ZnPhT/N-SMON nanoparticles are promising materials for PDT. Under dark conditions, cancer cells (HCP-116 cell line) maintained a cell viability of 89 ± 4% against up to 60 μg mL^{-1} of ZnPhT/N-SMON (Fig. 4c). In comparison, the cancer cell viability was gradually decreased up to 71 ± 2% under laser irradiation (4 J cm^{-2}) with 60 μg mL^{-1} of ZnPhT/N-SMON (Fig. 4d).

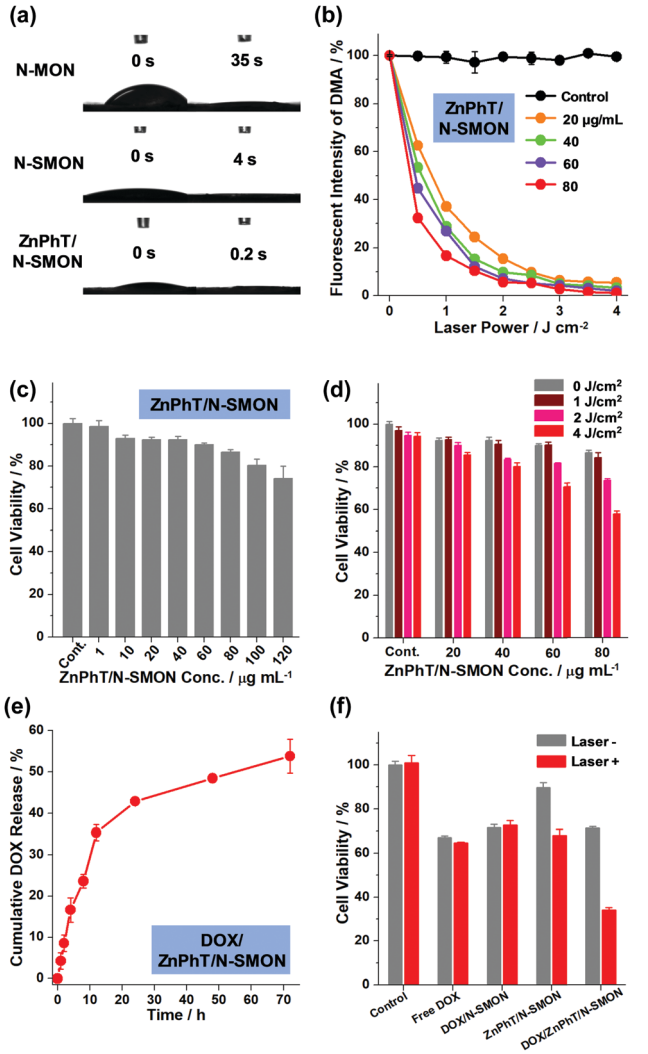

Fig. 4 (a) Water contact angles of N-MON, N-SMON, and ZnPhT/N-SMON. (b) Laser (λ = 671 nm)-induced singlet oxygen generation performance of ZnPhT/N-SMON based on the emission quenching of 9,10-dimethylanthracene (DMA) in DMF solution. (c) Cancer cell (HCP-116 cell line) viability depending on the concentration of ZnPhT/S-MON without laser irradiation. (d) Laser irradiation (λ = 671 nm) energy dependent PDT performance of ZnPhT/N-SMON for cancer cells. (e) DOX release behavior of DOX/ZnPhT/N-SMON (8.10 wt% DOX) in PBST (pH 7.4) buffer solution at 37 °C. (f) Cancer cell viability with DOX (5.0 μg mL^{-1}), DOX/N-SMON (55.1 μg mL^{-1}, 9.07 wt% DOX), ZnPhT/N-SMON (56.7 μg mL^{-1}), and DOX/ZnPhT/N-SMON (61.7 μg mL^{-1}, 8.10 wt% DOX) with/without laser irradiation (λ = 671 nm, irradiation energy of 4 J cm^{-2}).

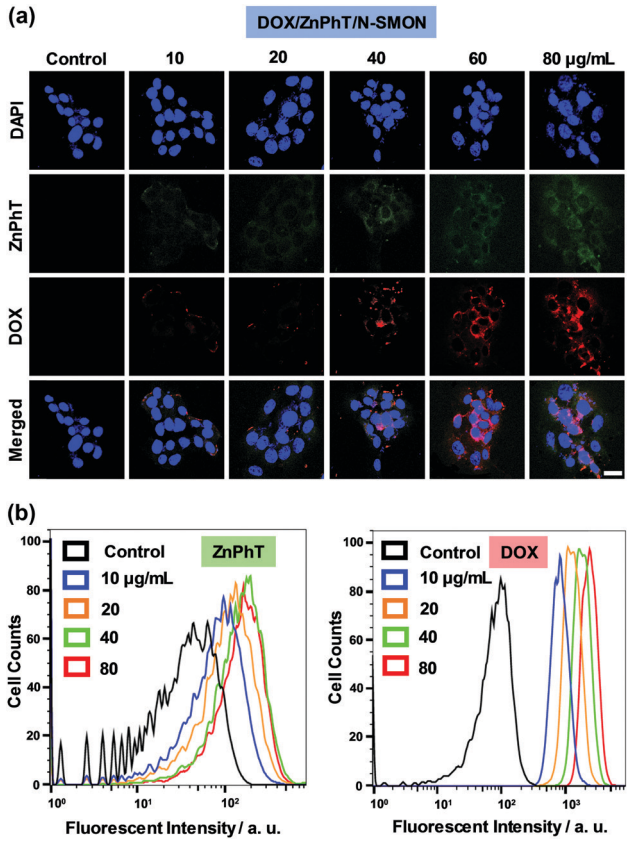

Fig. 5 (a) CLSM images of cancer cells (HCT-116 cell line) after treating with the DOX/ZnPhT/N-SMON (61.7 μg mL^{-1}) for 4 h (scale bar = 20 μm). (b) Flow cytometry of DOX/ZnPhT/N-SMON (HCT-116 cell counts = 1×10^5 cells per well, sample incubation time: 4 h, Alexa Fluor 647 dye for ZnPhT, PE dye for DOX).

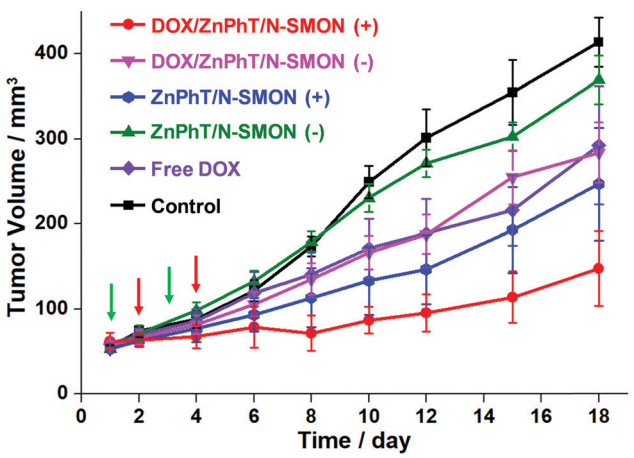

Fig. 6 *In vivo* tests (Balb/c mice, n = 5) for the inhibition of tumor growth by free DOX (2.5 mg kg^{-1}), ZnPhT/N-SMON (28.4 mg kg^{-1}), and DOX/ZnPhT/N-SMON (30.9 mg kg^{-1}) with/without laser irradiation. Green arrows: injection, red arrows: irradiation.

When we reduced the ZnPhT content in ZnPhT/N-SMON from 14.7 wt% to 7.4 and 3.7 wt%, the PDT activities gradually decreased, indicating that the PDT activities originated from the ZnPhT (Fig. S6 in the ESI†).

Next, we studied the DOX carrier ability of ZnPhT/N-SMON. When we treated the ZnPhT/N-SMON with DOX (a feed ratio of 10 : 1 = ZnPhT/N-SMON:DOX), the loaded amount of DOX was measured to be 8.10 wt%, corresponding to 88% drug loading efficiency (= [the amount of loaded DOX × 100]/initial amount of DOX). When we tested the DOX release behavior in PBS solution containing 0.1% Tween 20 (pH 7.4) at 37 °C, the 43 ± 1% and 54 ± 4% of DOX in the DOX/ZnPhT/N-SMON were released in 24 and 72 h, respectively (Fig. 4e).

As summarized in Fig. 4f, the dual therapeutic effect of DOX/ZnPhT/N-SMON *via* chemo-photodynamic therapy was studied.

In the control test without DOX/ZnPhT/N-SMON, the cancer cells survived completely with/without laser irradiation. When the free DOX (5.0 μg mL^{-1}) was used, there was no valid effect of laser irradiation with the cell viabilities of 65 ± 1 and 67 ± 1% with and without laser irradiation, respectively. The DOX/N-SMON (55.1 μg mL^{-1}, 9.07 wt% DOX) also showed no valid effect of laser irradiation with the cell viabilities of 73 ± 2 and 71 ± 2% with and without laser irradiation, respectively. Whereas ZnPhT/N-SMON (56.7 μg mL^{-1}) showed a decrease of cell viability to 68 ± 3% under laser irradiation, the cancer cells maintained a viability of 90 ± 1% without laser irradiation. On the other hand, while the DOX/ZnPhT/N-SMON (61.7 μg mL^{-1}, 8.10 wt% DOX) showed a cell viability of 71 ± 1% without laser irradiation, it showed an impressive decrease of cancer cell viability down to 34 ± 1% under laser irradiation, indicating that the dual photodynamic and chemotherapy of DOX/ZnPhT/N-SMON works efficiently in a synergistic way with an additional 9 ± 3% decrease of cancer cell viability, compared with the cases of DOX only or ZnPhT/N-SMON only.

The intracellular localization of DOX/ZnPhT/N-SMON nanoparticles was investigated by confocal laser scanning microscopy (CLSM) and flow cytometry (Fig. 5). According to the CLSM studies, the ZnPhT and DOX of DOX/ZnPhT/N-SMON was mostly detected in the cytoplasm of the cancer cells after an incubation time of 4 h (Fig. 5a). The relative intensities of the ZnPhT fluorescence gradually increased from 100% to 105, 126, and 144% with increasing concentrations of DOX/ZnPhT/N-SMON from 10 μg mL^{-1} to 20, 40, and 80 μg mL^{-1} (Fig. 5a and b). The relative intensities of the DOX fluorescence gradually increased from 100% to 158, 211, and 264% with increasing concentrations of DOX/ZnPhT/N-SMON from 10 μg mL^{-1} to 20, 40, and 80 μg mL^{-1} (Fig. 5a and b). These observations indicate the potential of the ZnPhT/N-SMON as a DOX carrier and a dual PDT and chemotherapy system for cancer cells.

To evaluate further the *in vivo* anticancer efficacy of combined PDT and chemotherapy with DOX/ZnPhT/N-SMON, the PBS solution, free DOX, ZnPhT/N-SMON, or DOX/ZnPhT/N-SMON (DOX dose, 2.5 mg kg^{-1}; ZnPhT dose, 4.2 mg kg^{-1}) were subcutaneously injected in duplicate at the tumor regions of mice bearing HCT-116 tumors, followed by laser irradiation.

In the cases of PBS solution and ZnPhT/N-SMON without laser irradiation, the tumor volumes increased continuously to ~350–400 mm^3 (Fig. 6). The cases of free DOX and DOX/ZnPhT/N-SMON without laser irradiation showed similar results with a decrease of tumor volume to ~250–300 mm^3, indicating that DOX in the carriers was efficiently delivered. Interestingly, ZnPhT/N-SMON and DOX/ZnPhT/N-SMON upon laser irradiation inhibited ~50% and ~75% of the tumor growth, respectively, compared to the case of PBS solution, due to the PDT effect. Over the animal tests, all mice showed negligible changes of body weights (Fig. S7 in the ESI†). Furthermore, there was no obvious damage in the major organs (Fig. S8 in the ESI†). These results indicate that the combined PDT and chemotherapy of DOX/ZnPhT/N-SMON could enhance the antitumor efficacy.

In conclusion, based on the MON chemistry, multifunctional drug delivery materials have been developed. Water-compatible N-MON nanoparticles were obtained through kinetic control of the growth of MON materials in the presence of PVP surfactant. Through introducing sulfonic acid groups to MON nanoparticles, ZnPhTs were anchored on the N-SMON nanoparticles through the coulombic interaction between sulfonate and cationic ZnPhT. In addition, DOX was loaded into the pores of the ZnPhT/N-SMON nanoparticles. The resultant DOX/ZnPhT/N-SMON nanoparticles showed water-compatibility and synergistic performance in dual photodynamic and chemotherapy towards cancer cells and tumors in *in vitro*/*vivo* tests. While the DOX/ZnPhT/N-SMON has no cancer targeting groups, we believe that the chemical surrounding and the functions of drug delivery systems can be further optimized through the variation of building blocks and post-functionalization.

Conflicts of interest

There are no conflicts to declare.

Acknowledgements

This work was supported by the Basic Science Research Program (2016R1E1A1A01941074 and NRF-2017R1A2B3010038) and Nano Material Technology Development Program (2018M3A7B4071235) through the National Research Foundation of Korea (NRF) funded by the Ministry of Science and ICT.

Notes and references

1 (*a*) N. Chaoui, M. Trunk, R. Dawson, J. Schmidt and A. Thomas, *Chem. Soc. Rev.*, 2017, **46**, 3302–3321; (*b*) L. Tan and B. Tan, *Chem. Soc. Rev.*, 2017, **46**, 3322–3356; (*c*) Y. Xu, S. Jin, H. Xu, A. Nagai and D. Jiang, *Chem. Soc. Rev.*, 2013, **42**, 8012–8031; (*d*) R. Dawson, A. I. Cooper and D. J. Adams, *Prog. Polym. Sci.*, 2012, **37**, 530–563; (*e*) F. Vilela, K. Zhang and M. Antonietti, *Energy Environ. Sci.*, 2012, **5**, 7819–7832; (*f*) D. Wu, F. Xu, B. Sun, R. Fu, H. He and K. Matyjaszewski, *Chem. Rev.*, 2012, **112**, 3959–4015; (*g*) N. B. McKeown and P. M. Budd, *Chem. Soc. Rev.*, 2006, **35**, 675–683.

2 (*a*) J.-X. Jiang, F. Su, A. Trewin, C. D. Wood, N. L. Campbell, H. Niu, C. Dickinson, A. Y. Ganin, M. J. Rosseinsky, Y. Z. Khimyak and A. I. Cooper, *Angew. Chem., Int. Ed.*, 2007, **46**, 8574–8578; (*b*) J.-X. Jiang, F. Su, A. Trewin, C. D. Wood, H. Niu, J. T. A. Jones, Y. Z. Khimyak and A. I. Cooper, *J. Am. Chem. Soc.*, 2008, **130**, 7710–7720.

3 J. Germain, J. M. J. Fréchet and F. Svec, *Small*, 2009, **5**, 1098–1111.

4 (*a*) B. Li, Z. Yang, L. Xia, M. I. Majeed and B. Tan, *Sci. Rep.*, 2013, **3**, 2128; (*b*) J. Tan, J. Wan, J. Guo and C. Wang, *Chem. Commun.*, 2015, **51**, 17394–17397; (*c*) Q. Li, S. Jin and B. Tan, *Sci. Rep.*, 2016, **6**, 31359; (*d*) J. Hynek, J. Rathousky, J. Demel and K. Lang, *RSC Adv.*, 2016, **6**, 44279–44287; (*e*) L. Wang, W. Wang, X. Zheng, Z. Li and Z. Xie, *Chem. – Eur. J.*, 2017, **23**, 1379–1385; (*f*) X. Zheng, L. Wang, Q. Pei, S. He, S. Liu

and Z. Xie, *Chem. Mater.*, 2017, **29**, 2374–2381; (*g*) Z. Li and Y.-W. Yang, *J. Mater. Chem. B*, 2017, **5**, 9278–9290; (*h*) S. Razzaque, C. Cai, Q.-W. Lu, F.-Z. Huang, Y.-S. Li, H.-B. Tang, I. Hussain and B. Tan, *J. Mater. Chem. B*, 2017, **5**, 742–749; (*i*) J. Y. Jang, H. T. T. Duong, S. M. Lee, H. J. Kim, Y.-J. Ko, J. H. Jeong, D. S. Lee, T. Thambi and S. U. Son, *Chem. Commun.*, 2018, **54**, 3652–3655; (*j*) J. Y. Jang, T. M. D. Le, J. H. Ko, Y.-J. Ko, S. M. Lee, H. J. Kim, J. H. Jeong, T. Thambi, D. S. Lee and S. U. Son, *Chem. Mater.*, 2019, **31**, 300–304.

5 (*a*) A. Li, H.-X. Sun, D.-Z. Tan, W.-J. Fan, S.-H. Wen, X.-J. Qing, G.-X. Li, S.-Y. Li and W.-Q. Deng, *Energy Environ. Sci.*, 2011, **4**, 2062–2065; (*b*) J. Chun, S. Kang, N. Park, E. J. Park, X. Jin, K.-D. Kim, H. O. Seo, S. M. Lee, H. J. Kim, W. H. Kwon, Y.-K. Park, J. M. Kim, Y. D. Kim and S. U. Son, *J. Am. Chem. Soc.*, 2014, **136**, 6786–6789.

6 (*a*) D. H. Lee, K. C. Ko, J. H. Ko, S. Y. Kang, S. M. Lee, H. J. Kim, Y.-J. Ko, J. Y. Lee and S. U. Son, *ACS Macro Lett.*, 2018, **7**, 651–655; (*b*) B. C. Ma, S. Ghasimi, K. Landfester, F. Vilela and K. A. I. Zhang, *J. Mater. Chem. A*, 2015, **3**, 16064–16071.

7 (*a*) P. Pallavi, S. Bandyopadhyav, J. Louis, A. Deshmukh and A. Patra, *Chem. Commun.*, 2017, **53**, 1257–1260; (*b*) K. Wu, J. Guo and C. Wang, *Chem. Commun.*, 2014, **50**, 695–697; (*c*) N. Kang, J. H. Park, M. Jin, N. Park, S. M. Lee, H. J. Kim, J. M. Kim and S. U. Son, *J. Am. Chem. Soc.*, 2013, **135**, 19115–19118; (*d*) A. Patra, J.-M. Koenen and U. Scherf, *Chem. Commun.*, 2011, **47**, 9612–9614.

8 (*a*) N. Kamaly, Z. Xiao, P. M. Valencia, A. F. Radovic-Moreno and O. C. Farokhzad, *Chem. Soc. Rev.*, 2012, **41**, 2971–3010; (*b*) Y. H. Bae and K. Park, *J. Controlled Release*, 2011, **153**, 198–205; (*c*) O. C. Farokhzad and R. Langer, *ACS Nano*, 2009, **3**, 16–20.

9 F. Fang, H. Nakamura and H. Maeda, *Adv. Drug Delivery Rev.*, 2011, **63**, 136–151.

10 (*a*) L. Xu, M. Zhao, Y. Yang, Y. Liang, C. Sun, W. Gao, S. Li, B. He and Y. A. Pu, *J. Mater. Chem. B*, 2017, **5**, 9157–9164; (*b*) W. Liu, Y.-M. Wang, Y.-H. Li, S.-J. Cai, X.-B. Yin, X.-W. He and Y.-K. Zhang, *Small*, 2017, **13**, 1603459; (*c*) Z. Wang, R. Ma, L. Yan, X. Chen and G. Zhu, *Chem. Commun.*, 2015, **51**, 11587–11590.

11 (*a*) M. C. DeRosa and R. J. Crutchley, *Coord. Chem. Rev.*, 2002, **233-234**, 351–371; (*b*) X. Ding and B.-H. Han, *Angew. Chem., Int. Ed.*, 2015, **54**, 6536–6539; (*c*) D. Cui, W. Xie, S. Zhang, Z. Liu, C. Liu and Y. Xu, *Mater. Lett.*, 2018, **232**, 18–21; (*d*) Y. Li, Q. Duan, H. Wang, B. Gao, N. Qiu and Y. Li, *J. Photochem. Photobiol., A*, 2018, **356**, 370–378; (*e*) L. Cai, Y. Li, Y. Li, H. Wang, Y. Yu, Y. Liu and Q. Duan, *J. Hazard. Mater.*, 2018, **348**, 47–55.

12 O. Tacar, P. Sriamornsak and C. R. Dass, *J. Pharm. Pharmacol.*, 2012, **65**, 157–170.

13 S. Yuan, S. Kirklin, B. Dorney, D.-J. Liu and L. Yu, *Macromolecules*, 2009, **42**, 1554–1559.

14 N. Park, Y. N. Lim, S. Y. Kang, S. M. Lee, H. J. Kim, Y.-J. Ko, B. Y. Lee, H.-Y. Jang and S. U. Son, *ACS Macro Lett.*, 2016, **5**, 1322–1326.

15 N. Park, D. Kang, M. C. Ahn, S. Kang, S. M. Lee, T. K. Ahn, J. Y. Jaung, H.-W. Shin and S. U. Son, *RSC Adv.*, 2015, **5**, 47270–47274.

16 I. Scalise and E. N. Durantini, *Bioorg. Med. Chem.*, 2005, **13**, 3037–3045.